Nano Research 2013, 6(9): 627–634
DOI 10.1007/s12274-013-0348-0
Research Article

ISSN 1998-0124
CN 11-5974/O4

Enhanced and tunable fluorescent quantum dots within a single crystal of protein

Hui Wei[1], Stephen House[2], Jiangjiexing Wu[1,3], Jiong Zhang[2], Zidong Wang[2], Ying He[2], Elizabeth J. Gao[1], Yigui Gao[4], Howard Robinson[5], Wei Li[3], Jianmin Zuo[2] (✉), Ian M. Robertson[2] (✉), and Yi Lu[1,2] (✉)

[1] *Department of Chemistry, University of Illinois at Urbana-Champaign, Illinois 61801, USA*
[2] *Department of Materials Science and Engineering, University of Illinois at Urbana-Champaign, Illinois 61801, USA*
[3] *Key Laboratory for Green Chemical Technology MOE, Tianjin University, Tianjin 300072, China*
[4] *George L. Clark X-Ray Facility and 3M Materials Laboratory, University of Illinois at Urbana-Champaign, Urbana, Illinois 61801, USA*
[5] *Department of Biology, Brookhaven National Laboratory, Upton, New York 11973, USA*

Received: 13 April 2013
Revised: 24 June 2013
Accepted: 8 July 2013

KEYWORDS
functional bio-nanomaterials, quantum dots, protein single crystals, X-ray crystallography, tomography

ABSTRACT

The design and synthesis of bio-nano hybrid materials can not only provide new materials with novel properties, but also advance our fundamental understanding of interactions between biomolecules and their abiotic counterparts. Here, we report a new approach to achieving such a goal by growing CdS quantum dots (QDs) within single crystals of lysozyme protein. This bio-nano hybrid emitted much stronger red fluorescence than its counterpart without the crystal, and such fluorescence properties could be either enhanced or suppressed by the addition of Ag(I) or Hg(II), respectively. The three-dimensional incorporation of CdS QDs within the lysozyme crystals was revealed by scanning transmission electron microscopy with electron tomography. More importantly, since our approach did not disrupt the crystalline nature of the lysozyme crystals, the metal and protein interactions were able to be studied by X-ray crystallography, thus providing insight into the role of Cd(II) in the CdS QDs formation.

1 Introduction

Bio-nanomaterials combine the merits of both biomolecules and nanomaterials, and have found applications in many areas, from catalysis, energy conversion and storage, to artificial tissues, sensing, imaging, and drug delivery [1–10]. To achieve the goal of preparing hybrid materials, many biomolecules such as DNA, proteins, carbohydrate, viruses, and bacteria have been explored [11–27]. Among them, proteins have been successfully utilized to construct a variety of bio-nanomaterials due to their nanoscale sizes comparable to most nanomaterials, their structural and functional diversities, and their recognition and assembly capabilities [28–37]. Most previous research, however, has focused on proteins in solution as

Address correspondence to Yi Lu, yi-lu@illinois.edu; Ian M. Robertson, ianr@illinois.edu; Jianmin Zuo, jianzuo@illinois.edu

templates for nanomaterial synthesis; for example, caged proteins have been employed as nanocontainers for directing preparation of nanomaterials in solution [38–40]. Protein single crystals, on the other hand, have highly-ordered three-dimensional structures and thus can be regarded as porous materials [41, 42]. The unique characteristics of protein crystals, such as three-dimensional assemblies at both macroscale and nanoscale, and nanosized porous structures, allows controlled growth of nanomaterials on a time scale by which the kinetics and mechanism of the growth can be readily studied using microscopic methods. Although the synthesis and characterization of nanomaterials within protein single crystals have been recently reported [42–50], this method's full potential has not been reached, especially for those reagents and conditions that do not disrupt the crystalline lattice. This latter feature is especially important for high-resolution three-dimensional structural study of the protein interactions with metal ions during the nanomaterials growth.

We have recently reported the synthesis and characterization of gold nanoparticles (AuNPs) grown within intact lysozyme single crystals [46]. Because the protein single crystals provided a well-defined three-dimensional matrix where each protein inside the crystal can be studied at an atomic level by X-ray crystallography, we were able to reveal mechanisms of AuNP formation directed by the protein template. Given the initial success, we wondered whether such an approach can be applied to synthesize and study other nanomaterials within single protein crystals. Quantum dots (QDs) are promising inorganic nanomaterials that have been studied extensively during the past decades due to their unique optical properties for use in areas such as bioimaging, optoelectronic devices, and solar cells [51–66]. Growing QDs within the intact protein single crystals will allow us to study not only the mechanism of the QDs formation directed by the protein, but also the influence of the protein crystals on the optical properties of QDs. In this study, we demonstrate that CdS QDs can be formed *in situ* within single crystals of proteins, resulting in fluorescent nanomaterial-in-crystal hybrids. We also show that the fluorescence properties of the hybrids can be fine-tuned by the addition of selected chemical species.

2 Results and discussion

The CdS QDs within the lysozyme single crystals (called CdS@Lysozyme) were prepared by growing the crystals from cadmium acetate, sodium sulfide, and lysozyme at room temperature. The crystals of CdS@Lysozyme could be observed after about one day of growth. As shown in Fig. 1, the crystals were yellow in color and emitted red fluorescence with a peak centered at ~700 nm under fluorescein isothiocyanate (FITC) (~450–500 nm) illumination (also see Fig. S1 (in the Electronic Supplementary Material (ESM)). This Stokes-shifted emission band of 700 nm was due to the trapped charge carriers' radiative recombination [67]. In contrast, when the crystals were grown under the same conditions but in the absence of sodium sulfide, the crystals of Cd(II)@Lysozyme were colorless and non-fluorescent. These results suggest that the color and fluorescence may be due to the formation of CdS QDs inside the protein crystals.

Although CdS QDs have been synthesized, only limited reports have demonstrated fluorescence properties of biosynthesized CdS QDs in aqueous solution, partly due to the intrinsically weak fluorescence from the CdS QDs' broad trap emission [68–71]. For example, as a control experiment, when CdS QDs were synthesized in the buffer solution containing lysozyme under conditions that no crystal was formed, little red fluorescence emission was observed (Fig. S2 (in the ESM)). Moreover, when the as-prepared CdS@Lysozyme crystals were re-dissolved in buffer solution, red fluorescence emission disappeared (Fig. S3 (in the ESM)). Instead, insoluble yellow-colored aggregates were observed in both control experiments described above. To enhance the crystal stability in buffers, glutaraldehyde can be used to cross-link the crystals [44], and such cross-linked crystals containing Au nanoparticles have shown interesting catalytic properties in solution [49]. These results suggest that the protein crystals provided a unique microenvironment for formation of CdS QDs with enhanced fluorescence properties.

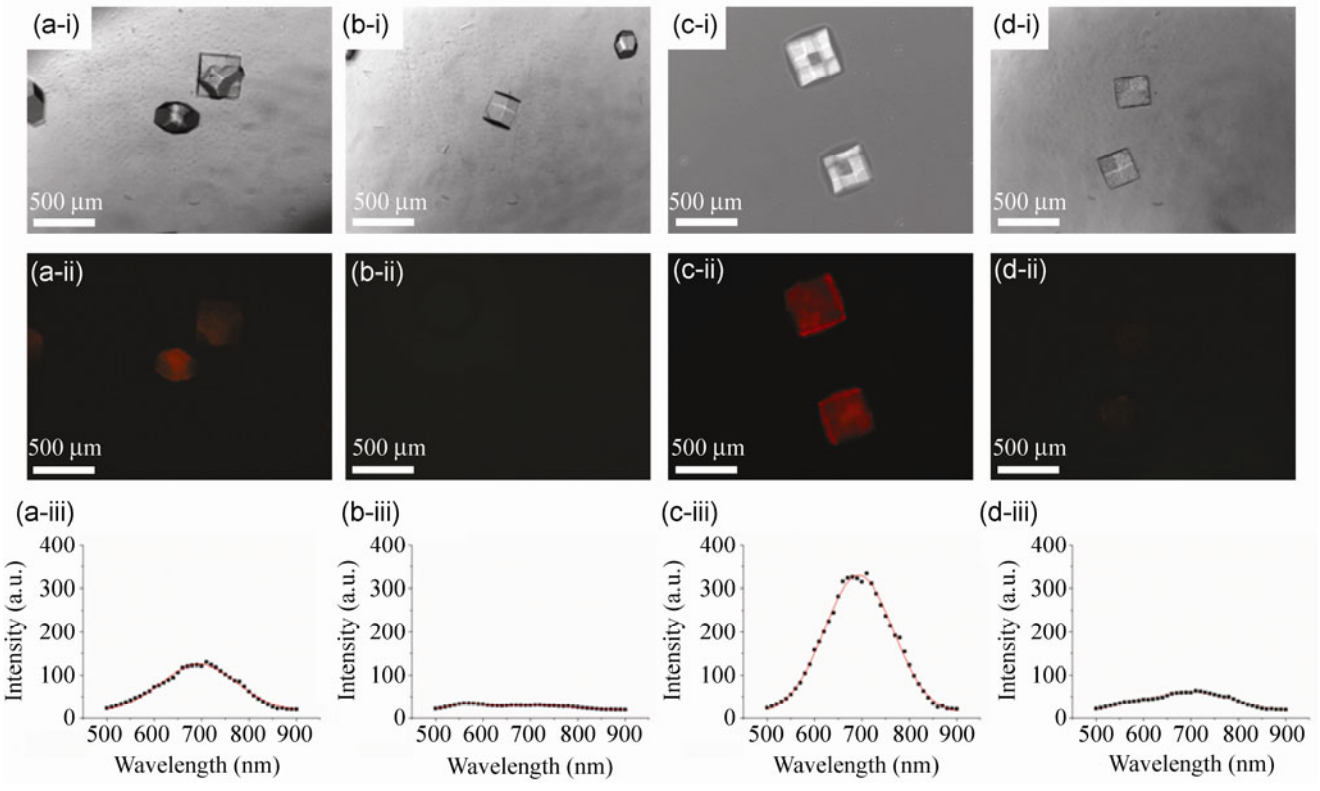

Figure 1 Bright field (i), fluorescence images (ii), and emission spectra (iii) of lysozyme single crystals. From left to right: CdS@Lysozyme (a), Cd(II)@Lysozyme (b), CdS@Lysozyme with Ag(I) (c), and CdS@Lysozyme with Hg(II) (d). The fluorescence images were collected on a Nuance multispectral imaging system with a fluorescein isothiocyanate (FITC) filter for excitation and a long pass filter for emission. Exposure time = 500 ms.

To verify that the CdS QDs were indeed formed within the lysozyme crystals, we used electron microscopy to study the as-prepared CdS@Lysozyme. After 8 days of growth, the size of the QDs within the lysozyme crystals was found to be ~9.8 ± 2.2 nm (Fig. 2). To further characterize the chemical composition of the CdS@Lysozyme, single-particle energy-dispersive X-ray spectrum (EDS) analysis was carried out (Fig. S4 (in the ESM)). The peaks of Cd, S, Cl, C, and Cu were present, confirming the formation of CdS QDs (the peak of Cl originated from the NaCl in the crystallization buffer and the peaks of C and Cu originated from the transmission electron microscopy (TEM) grid, respectively).

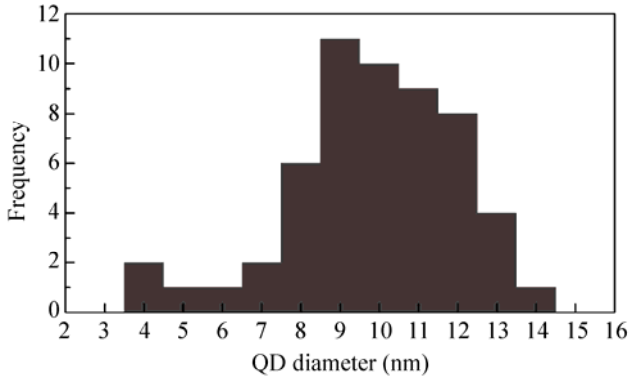

Figure 2 Size distribution of CdS QDs in the crystal used for the tomographic study. The diameters were measured from the source micrographs in the tilt series.

To determine the locations of the CdS QDs entrapped within the lysozyme single crystals, we performed an electron tomographic study. Electron tomography, an emerging technique for three-dimensional imaging [72, 73], enables us to visualize how the small objects are distributed three-dimensionally in the matrix. High-angle annular-dark-field scanning transmission electron microscopy (HAADF-STEM) was used to collect a series of images at different tilt angles for tomographic reconstruction due to its effective suppression of coherent diffraction and Z-contrast imaging

mechanism [73]. Because the Z difference between the CdS QDs and the lysozyme protein matrix is large enough, the contrast is sufficient to distinguish between them in a tomographic reconstruction. A tilt series of a relatively thin sample area was acquired over ± 44°, with an image taken every 2°, and used to construct a tomogram. Movies of the aligned tilt series and the reconstructed tomogram are included in the ESM as Alignment and Reconstruction, respectively. Figure 3(a) shows a single HAADF-STEM image of CdS QDs within the lysozyme single crystals at 0° tilt. Figure 3(b) is a cross-sectional slice through the reconstructed tomogram, demonstrating how the three-dimensional reconstruction clearly reveals the CdS QDs to be inside the lysozyme crystal. Figures 3(c) and 3(d) are the corresponding images to Fig. 3(a) from the tomogram. The CdS QDs in Fig. 3(a) overlays well with those in Figs. 3(c) and 3(d), supporting the fidelity of the reconstruction.

To quantify the encapsulation, the depth of each CdS QD inside the lysozyme crystal was measured from the reconstructed tomogram (Fig. 4). The depth

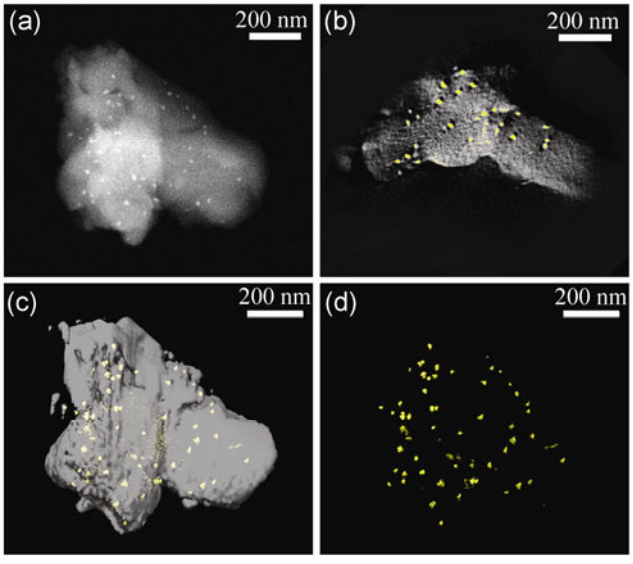

Figure 3 HAADF-STEM image of CdS@Lysozyme single crystals at 0° tilt (a) and the corresponding snapshot from the three-dimensional tomographic reconstruction (c). (d) is the same snapshot as (c) without lysozyme. (b) is a cross-sectional slice through the reconstructed tomogram. In (a), the white dots show the CdS quantum dots incorporated within the lysozyme matrix, which is slightly darker. In (b)–(d), the CdS quantum dots are yellow; the lysozyme crystals are white.

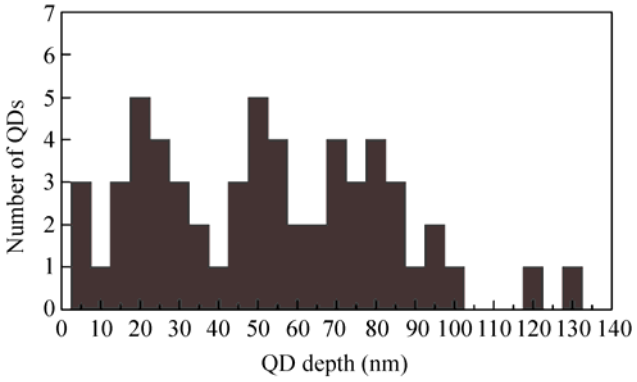

Figure 4 Distribution of depths below the lysozyme crystal's surface of the CdS QDs. Depths were measured from the center of the QD to the nearest surface.

distribution appeared rather uniform throughout the crystal, with no strong preference for any particular depth. No QDs were observed outside the lysozyme surface; at their shallowest, the QDs were flush with the surface, and even then only three of the 58 QDs were this close to the surface. The vast majority was entirely encapsulated within the crystal to a depth of multiple QD diameters. Only two QDs were observed at a depth > 100 nm because there were very few regions of the crystal that were > 100 nm from any surface.

Remarkably, despite the encapsulation of hundreds of CdS QDs within the protein matrix, the lysozyme single crystals remained intact, resulting in X-ray diffraction patterns similar to those of lysozyme alone. This feature allowed us to study the Cd(II) ions' binding sites in the protein and to elucidate its role in directing the CdS QDs growth by using high-resolution X-ray crystallography. Figure 5 shows the high-resolution X-ray crystallographic structures of Cd(II)@Lysozyme and CdS@Lysozyme obtained. Nine Cd^{2+} ions were observed in the crystal structure of Cd(II)@Lysozyme.

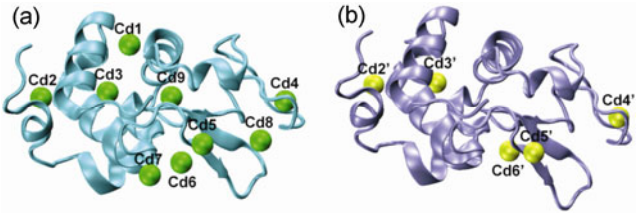

Figure 5 X-ray crystallographic structures of Cd(II)@Lysozyme (a) and CdS@Lysozyme (b). Cd^{2+} ions are shown as balls.

One Cd^{2+} ion, named Cd1, was coordinated by the ε-N of His15; the same residue was involved in coordination with a Au(I) ion in a previously reported AuNP@Lysozyme [46]. The other eight Cd^{2+} ions, Cd2 to Cd9, interacted with N (or O) atoms of several residues, such as Tyr23, Ser24, Phe34, Gln41, Thr43, Gly49, Thr51, Asp52, Tyr53, Leu56, Gln57, Asn65, Asp66, Arg68, Thr69, Ser72, and Ser91 (see Fig. S5 (in the ESM) for detailed binding motifs). In the case of CdS@Lysozyme, however, only five Cd^{2+} ions, Cd2′ to Cd6′, were observed, which bound to N (or O) atoms of Tyr23, Ser24, Gln41, Thr43, Asp52, Gln57, Asn65, Thr69, and Ser72 (see Fig. S6 (in the ESM) for detailed binding motifs). These five Cd^{2+} ions have almost identical binding sites as Cd2 to Cd6 of Cd(II)@Lysozyme. The other four Cd^{2+} ions, Cd1, and Cd7 to Cd9, of Cd(II)@Lysozyme initially bound to His15 while other residues disappeared when CdS QDs formed. These results indicate that the binding of Cd(II) ions to His15 and several other residues (i.e., Phe34, Gly49, Thr51, Tyr53, Leu56, Asp66, Arg68, and Ser91) may direct the growth of CdS QDs.

To demonstrate control of the fluorescence properties of CdS@Lysozyme, we added different metal ions. Interestingly, we found that Ag(I) ions enhanced the fluorescence emission of CdS@Lysozyme crystals significantly (Fig. 1(c)), while Hg(II) ions quenched the fluorescence emission (Fig. 1(d)). The enhancement of fluorescence emission by Ag(I) ions could be due to the formation of new radiative centers and the blocking of nonradiative defect sites on the CdS QDs' surface [74], while the quenching induced by Hg(II) ions could originate from their binding to the CdS QDs' surface and further electron transfer from surface traps of QDs to Hg(II) ions [75]. To further confirm the enhancement or suppression of the fluorescence intensity of the CdS@Lysozyme, we added 1.5 μL and 3 μL of 1 mM Ag(I) to the solution containing the CdS@Lysozyme. As shown in Fig. S7 (in the ESM), increased enhancements of fluorescence intensity were observed with increasing concentrations of the Ag(I). Similarly, addition of increasing concentrations of Hg(II) caused a decrease in fluorescence intensity of the crystals. These results suggest that it is possible to fine-tune the fluorescence properties of CdS@Lysozyme hybrids by using additional chemical species.

3 Conclusions

We have developed an approach to prepare CdS QDs within lysozyme single crystals without disturbing the protein crystalline lattice. Fluorescence imaging showed that the as-prepared hybrids could emit red fluorescence. The fluorescence properties of the hybrids could be further fine-tuned by additional different metal ions. The CdS QDs' three-dimensional distribution and the cadmium ions' interactions with lysozyme were revealed by STEM with tomography and X-ray crystallography, respectively. This study may provide a new approach to synthesize functional nanomaterial-in-crystal hybrids, which could find potential applications in catalysis, optical and plasmonic devices, and stimuli-responsive materials. It also allows us to further understand the chemistry of biomineralization, and the interactions between biomolecules and nanomaterials.

Acknowledgements

This work was supported by the US National Science Foundation (Nos. CMMI 0749028 and DMR-0117792). The authors thank C. Lei and W. Swiech for help with the STEM imaging, C. M. Bee and D. Zhang for fluorescence microscopic measurements, S. M. Nie for the use of Nuance system and A. M. Smith for insightful discussions. S. H. and I. M. R. acknowledge support from the US Department of Energy (grant No. DE-FC36-05GO15064). STEM experiments were carried out in part in the Frederick Seitz Materials Research Laboratory Central Facilities, University of Illinois. X-ray crystallographic data for this study were measured at beamline X12C of the National Synchrotron Light Source, Brookhaven National Laboratory. Financial support comes principally from the Offices of Biological and Environmental Research and of Basic Energy Sciences of the US Department of Energy, and from the National Center for Research Resources (No. P41RR012408) and the National Institute of General Medical Sciences (No. P41GM103473) of the National Institutes of Health.

Electronic Supplementary Material: Supplementary material (experimental details, additional figures and

movies, and X-ray crystallographic data) is available in the online version of this article at http://dx.doi.org/10.1007/s12274-013-0348-0.

References

[1] Niemeyer, C. M.; Mirkin, C. A. *Nanobiotechnology II: More concepts and applications*; WILEY-VCH: Weinheim, 2004.

[2] Xue, X. J.; Wang, F.; Liu, X. G. One-step, room temperature, colorimetric detection of mercury (Hg^{2+}) using DNA/nanoparticle conjugates. *J. Am. Chem. Soc.* **2008**, *130*, 3244–3245.

[3] Suzuki, M.; Abe, M.; Ueno, T.; Abe, S.; Goto, T.; Toda, Y.; Akita, T.; Yamadae, Y.; Watanabe, Y. Preparation and catalytic reaction of Au/Pd bimetallic nanoparticles in Apo-ferritin. *Chem. Commun.* **2009**, 4871–4873.

[4] Ruiz-Hitzky, E.; Darder, M.; Aranda, P.; Ariga, K. Advances in biomimetic and nanostructured biohybrid materials. *Adv. Mater.* **2010**, *22*, 323–336.

[5] Wang, F.; Tan, W. B.; Zhang, Y.; Fan, X. P.; Wang, M. Q. Luminescent nanomaterials for biological labelling. *Nanotechnology* **2006**, *17*, R1–R13.

[6] Yan, J. L.; Estevez, M. C.; Smith, J. E.; Wang, K. M.; He, X. X.; Wang, L.; Tan, W. H. Dye-doped nanoparticles for bioanalysis. *Nano Today* **2007**, *2*, 44–50.

[7] Lu, Y.; Liu, J. W. Smart nanomaterials inspired by biology: Dynamic assembly of error-free nanomaterials in response to multiple chemical and biological stimuli. *Acc. Chem. Res.* **2007**, *40*, 315–323.

[8] Wang, Z. D.; Lu, Y. Functional DNA directed assembly of nanomaterials for biosensing. *J. Mater. Chem.* **2009**, *19*, 1788–1798.

[9] Lee, J. H.; Yigit, M. V.; Mazumdar, D.; Lu, Y. Molecular diagnostic and drug delivery agents based on aptamer-nanomaterial conjugates. *Adv. Drug Deliv. Rev.* **2010**, *62*, 592–605.

[10] Xing, H.; Wong, N. Y.; Xiang, Y.; Lu, Y. DNA aptamer functionalized nanomaterials for intracellular analysis, cancer cell imaging and drug delivery. *Curr. Opin. Chem. Biol.* **2012**, *16*, 429–435.

[11] Pal, S.; Sharma, J.; Yan, H.; Liu, Y. Stable silver nanoparticle-DNA conjugates for directed self-assembly of core–satellite silver–gold nanoclusters. *Chem. Commun.* **2009**, 6059–6061.

[12] Choi, S.; Dickson, R. M.; Yu, J. Developing luminescent silver nanodots for biological applications. *Chem. Soc. Rev.* **2012**, *41*, 1867–1891.

[13] Dickerson, M. B.; Sandhage, K. H.; Naik, R. R. Protein- and peptide-directed syntheses of inorganic materials. *Chem. Rev.* **2008**, *108*, 4935–4978.

[14] Sanders, L. K.; Xian, W. J.; Guaqueta, C.; Strohman, M. J.; Vrasich, C. R.; Luijten, E.; Wong, G. C. L. Control of electrostatic interactions between F-actin and genetically modified lysozyme in aqueous media. *Proc. Natl. Acad. Sci. U. S. A.* **2007**, *104*, 15994–15999.

[15] Zhang, M. G.; Smith, A.; Gorski, W. Carbon nanotube-chitosan system for electrochemical sensing based on dehydrogenase enzymes. *Anal. Chem.* **2004**, *76*, 5045–5050.

[16] Lee, Y. J.; Yi, H.; Kim, W. J.; Kang, K.; Yun, D. S.; Strano, M. S.; Ceder, G.; Belcher, A. M. Fabricating genetically engineered high-power lithium-ion batteries using multiple virus genes. *Science* **2009**, *324*, 1051–1055.

[17] Park, T. J.; Lee, S. Y.; Heo, N. S.; Seo, T. S. *In vivo* synthesis of diverse metal nanoparticles by recombinant *Escherichia coli*. *Angew. Chem. Int. Ed.* **2010**, *49*, 7019–7024.

[18] Sturzenbaum, S. R.; Hockner, M.; Panneerselvam, A.; Levitt, J.; Bouillard, J. S.; Taniguchi, S.; Dailey, L. A.; Khanbeigi, R. A.; Rosca, E. V.; Thanou, M. et al. Biosynthesis of luminescent quantum dots in an earthworm. *Nat. Nanotechnol.* **2013**, *8*, 57–60.

[19] Bao, H. F.; Lu, Z. S.; Cui, X. Q.; Qiao, Y.; Guo, J.; Anderson, J. M.; Li, C. M. Extracellular microbial synthesis of biocompatible CdTe quantum dots. *Acta Biomater.* **2010**, *6*, 3534–3541.

[20] Liu, J. W.; Lu, Y. A colorimetric lead biosensor using DNAzyme-directed assembly of gold nanoparticles. *J. Am. Chem. Soc.* **2003**, *125*, 6642–6643.

[21] Wei, H.; Wang, Z. D.; Yang, L. M.; Tian, S. L.; Hou, C. J.; Lu, Y. Lysozyme-stabilized gold fluorescent cluster: Synthesis and application as Hg^{2+} sensor. *Analyst* **2010**, *135*, 1406–1410.

[22] Xing, H.; Wang, Z. D.; Xu, Z. D.; Wong, N. Y.; Xiang, Y.; Liu, G. L. G.; Lu, Y. DNA-directed assembly of asymmetric nanoclusters using Janus nanoparticles. *ACS Nano* **2012**, *6*, 802–809.

[23] Li, L. L.; Zhang, R. B.; Yin, L. L.; Zheng, K. Z.; Qin, W. P.; Selvin, P. R.; Lu, Y. Biomimetic surface engineering of lanthanide-doped upconversion nanoparticles as versatile bioprobes. *Angew. Chem. Int. Ed.* **2012**, *51*, 6121–6125.

[24] Li, L. L.; Yin, Q.; Cheng, J. J.; Lu, Y. Polyvalent mesoporous silica nanoparticle-aptamer bioconjugates target breast cancer cells. *Adv. Healthcare Mater.* **2012**, *1*, 567–572.

[25] Wang, Z. D.; Tang, L. H.; Tan, L. H.; Li, J. H.; Lu, Y. Discovery of the DNA "genetic code" for abiological gold nanoparticle morphologies. *Angew. Chem. Int. Ed.* **2012**, *51*, 9078–9082.

[26] Wu, P. W.; Hwang, K.; Lan, T.; Lu, Y. A DNAzyme-gold nanoparticle probe for uranyl ion in living cells. *J. Am. Chem. Soc.* **2013**, *135*, 5254–5257.

[27] Li, L. L.; Wu, P. W.; Hwang, K.; Lu, Y. An exceptionally

simple strategy for DNA-functionalized up-conversion nanoparticles as biocompatible agents for nanoassembly, DNA delivery, and imaging. *J. Am. Chem. Soc.* **2013**, *135*, 2411–2414.

[28] Ueno, T.; Abe, S.; Yokoi, N.; Watanabe, Y. Coordination design of artificial metalloproteins utilizing protein vacant space. *Coord. Chem. Rev.* **2007**, *251*, 2717–2731.

[29] Xie, J. P.; Zheng, Y. G.; Ying, J. Y. Protein-directed synthesis of highly fluorescent gold nanoclusters. *J. Am. Chem. Soc.* **2009**, *131*, 888–889.

[30] Medalsy, I.; Dgany, O.; Sowwan, M.; Cohen, H.; Yukashevska, A.; Wolf, S. G.; Wolf, A.; Koster, A.; Almog, O.; Marton, I. et al. SP1 protein-based nanostructures and arrays. *Nano Lett.* **2008**, *8*, 473–477.

[31] Dani, R. K.; Kang, M.; Kalita, M.; Smith, P. E.; Bossmann, S. H.; Chikan, V. MspA porin–gold nanoparticle assemblies: Enhanced binding through a controlled cysteine mutation. *Nano Lett.* **2008**, *8*, 1229–1236.

[32] Guo, C. L.; Irudayaraj, J. Fluorescent Ag clusters via a protein-directed approach as a Hg(II) ion sensor. *Anal. Chem.* **2011**, *83*, 2883–2889.

[33] Chaudhari, K.; Xavier, P. L.; Pradeep, T. Understanding the evolution of luminescent gold quantum clusters in protein templates. *ACS Nano* **2011**, *5*, 8816–8827.

[34] Ge, J.; Lei, J. D.; Zare, R. N. Protein–inorganic hybrid nanoflowers. *Nat. Nanotechnol.* **2012**, *7*, 428–432.

[35] Wang, Y. C.; Wang, Y.; Zhou, F. B.; Kim, P.; Xia, Y. N. Protein-protected Au clusters as a new class of nanoscale biosensor for label-free fluorescence detection of proteases. *Small* **2012**, *8*, 3769–3773.

[36] Colombo, M.; Mazzucchelli, S.; Collico, V.; Avvakumova, S.; Pandolfi, L.; Corsi, F.; Porta, F.; Prosperi, D. Protein-assisted one-pot synthesis and biofunctionalization of spherical gold nanoparticles for selective targeting of cancer cells. *Angew. Chem. Int. Ed.* **2012**, *51*, 9272–9275.

[37] Chen, T. H.; Tseng, W. L. (Lysozyme type VI)-stabilized Au8 clusters: Synthesis mechanism and application for sensing of glutathione in a single drop of blood. *Small* **2012**, *8*, 1912–1919.

[38] Meldrum, F. C.; Wade, V. J.; Nimmo, D. L.; Heywood, B. R.; Mann, S. Synthesis of inorganic nanophase materials in supramolecular protein cages. *Nature* **1991**, *349*, 684–687.

[39] Uchida, M.; Klem, M. T.; Allen, M.; Suci, P.; Flenniken, M.; Gillitzer, E.; Varpness, Z.; Liepold, L. O.; Young, M.; Douglas, T. Biological containers: Protein cages as multifunctional nanoplatforms. *Adv. Mater.* **2007**, *19*, 1025–1042.

[40] Butts, C. A.; Swift, J.; Kang, S. G.; Di Costanzo, L.; Christianson, D. W.; Saven, J. G.; Dmochowski, I. J. Directing noble metal ion chemistry within a designed ferritin protein. *Biochemistry* **2008**, *47*, 12729–12739.

[41] Margolin, A. L.; Navia, M. A. Protein crystals as novel catalytic materials. *Angew. Chem. Int. Ed.* **2001**, *40*, 2204–2222.

[42] Sanghamitraa, N. J. M.; Ueno, T. Expanding coordination chemistry from protein to protein assembly. *Chem. Commun.* **2013**, *49*, 4114–4126.

[43] Falkner, J. C.; Turner, M. E.; Bosworth, J. K.; Trentler, T. J.; Johnson, J. E.; Lin, T. W.; Colvin, V. L. Virus crystals as nanocomposite scaffolds. *J. Am. Chem. Soc.* **2005**, *127*, 5274–5275.

[44] Guli, M.; Lambert, E. M.; Li, M.; Mann, S. Template-directed synthesis of nanoplasmonic arrays by intracrystalline metalization of cross-linked lysozyme crystals. *Angew. Chem. Int. Ed.* **2010**, *49*, 520–523.

[45] Ueno, T.; Abe, S.; Koshiyama, T.; Ohki, T.; Hikage, T.; Watanabe, Y. Elucidation of metal-ion accumulation induced by hydrogen bonds on protein surfaces by using porous lysozyme crystals containing Rh-III ions as the model surfaces. *Chem. Eur. J.* **2010**, *16*, 2730–2740.

[46] Wei, H.; Wang, Z. D.; Zhang, J.; House, S.; Gao, Y. G.; Yang, L. M.; Robinson, H.; Tan, L. H.; Xing, H.; Hou, C. J. et al. Time-dependent, protein-directed growth of gold nanoparticles within a single crystal of lysozyme. *Nat. Nanotechnol.* **2011**, *6*, 93–97.

[47] Vekilov, P. G. Gold nanoparticles grown in a crystal. *Nat. Nanotechnol.* **2011**, *6*, 82–83.

[48] Liu, C. L.; Wu, H. T.; Hsiao, Y. H.; Lai, C. W.; Shih, C. W.; Peng, Y. K.; Tang, K. C.; Chang, H. W.; Chien, Y. C.; Hsiao, J. K. et al. Insulin-directed synthesis of fluorescent gold nanoclusters: Preservation of insulin bioactivity and versatility in cell imaging. *Angew. Chem. Int. Ed.* **2011**, *50*, 7056–7060.

[49] Wei, H.; Lu, Y. Catalysis of gold nanoparticles within lysozyme single crystals. *Chem. Asian J.* **2012**, *7*, 680–683.

[50] Abe, S.; Tsujimoto, M.; Yoneda, K.; Ohba, M.; Hikage, T.; Takano, M.; Kitagawa, S.; Ueno, T. Porous protein crystals as reaction vessels for controlling magnetic properties of nanoparticles. *Small* **2012**, *8*, 1314–1319.

[51] Steigerwald, M. L.; Brus, L. E. Semiconductor crystallites: A class of large molecules. *Acc. Chem. Res.* **1990**, *23*, 183–188.

[52] Chan, W. C. W.; Nie, S. M. Quantum dot bioconjugates for ultrasensitive nonisotopic detection. *Science* **1998**, *281*, 2016–2018.

[53] Bruchez, M.; Moronne, M.; Gin, P.; Weiss, S.; Alivisatos, A. P. Semiconductor nanocrystals as fluorescent biological labels. *Science* **1998**, *281*, 2013–2016.

[54] Bhattacharya, P.; Ghosh, S.; Stiff-Roberts, A. D. Quantum dot opto-electronic devices. *Ann. Rev. Mater. Res.* **2004**, *34*, 1–40.

[55] Gao, X. H.; Cui, Y. Y.; Levenson, R. M.; Chung, L. W. K.; Nie, S. M. *In vivo* cancer targeting and imaging with semiconductor quantum dots. *Nat. Biotechnol.* **2004**, *22*, 969–976.

[56] Sargent, E. H. Colloidal quantum dot solar cells. *Nat. Photonics* **2012**, *6*, 133–135.

[57] Regulacio, M. D.; Han, M. Y. Composition-tunable alloyed semiconductor nanocrystals. *Acc. Chem. Res.* **2010**, *43*, 621–630.

[58] Peng, X. G.; Manna, L.; Yang, W. D.; Wickham, J.; Scher, E.; Kadavanich, A.; Alivisatos, A. P. Shape control of CdSe nanocrystals. *Nature* **2000**, *404*, 59–61.

[59] Li, Z.; Qin, H. Y.; Guzun, D.; Benamara, M.; Salamo, G.; Peng, X. G. Uniform thickness and colloidal-stable CdS quantum disks with tunable thickness: Synthesis and properties. *Nano Res.* **2012**, *5*, 337–351.

[60] Li, F.; Zhang, Z. P.; Peng, J.; Cui, Z. Q.; Pang, D. W.; Li, K.; Wei, H. P.; Zhou, Y. F.; Wen, J. K.; Zhang, X. E. Imaging viral behavior in mammalian cells with self-assembled capsid-quantum-dot hybrid particles. *Small* **2009**, *5*, 718–726.

[61] Hu, M.; Yan, J.; He, Y.; Lu, H. T.; Weng, L. X.; Song, S. P.; Fan, C. H.; Wang, L. H. Ultrasensitive, multiplexed detection of cancer biomarkers directly in serum by using a quantum dot-based microfluidic protein chip. *ACS Nano* **2010**, *4*, 488–494.

[62] Xiao, Q.; Huang, S.; Qi, Z. D.; Zhou, B.; He, Z. K.; Liu, Y. Conformation, thermodynamics and stoichiometry of HSA adsorbed to colloidal CdSe/ZnS quantum dots. *BBA-Proteins Proteomics* **2008**, *1784*, 1020–1027.

[63] Chen, L. D.; Liu, J.; Yu, X. F.; He, M.; Pei, X. F.; Tang, Z. Y.; Wang, Q. Q.; Pang, D. W.; Li, Y. The biocompatibility of quantum dot probes used for the targeted imaging of hepatocellular carcinoma metastasis. *Biomaterials* **2008**, *29*, 4170–4176.

[64] Qu, Y.; Li, W.; Zhou, Y. L.; Liu, X. F.; Zhang, L. L.; Wang, L. M.; Li, Y. F.; Iida, A.; Tang, Z. Y.; Zhao, Y. L. et al. Full assessment of fate and physiological behavior of quantum dots utilizing caenorhabditis elegans as a model organism. *Nano Lett.* **2011**, *11*, 3174–3183.

[65] Kang, Z. H.; Liu, Y.; Tsang, C. H. A.; Ma, D. D. D.; Fan, X.; Wong, N. B.; Lee, S. T. Water-soluble silicon quantum dots with wavelength-tunable photoluminescence. *Adv. Mater.* **2009**, *21*, 661–664.

[66] Liu, J. W.; Lee, J. H.; Lu, Y. Quantum dot encoding of aptamer-linked nanostructures for one-pot simultaneous detection of multiple analytes. *Anal. Chem.* **2007**, *79*, 4120–4125.

[67] Resch, U.; Eychmuller, A.; Haase, M.; Weller, H. Absorption and fluorescence behavior of redispersible Cds colloids in various organic-solvents. *Langmuir* **1992**, *8*, 2215–2218.

[68] Dameron, C. T.; Reese, R. N.; Mehra, R. K.; Kortan, A. R.; Carroll, P. J.; Steigerwald, M. L.; Brus, L. E.; Winge, D. R. Biosynthesis of cadmium-sulfide quantum semiconductor crystallites. *Nature* **1989**, *338*, 596–597.

[69] Wong, K. K. W.; Mann, S. Biomimetic synthesis of cadmium sulfide-ferritin nanocomposites. *Adv. Mater.* **1996**, *8*, 928–932.

[70] Naito, M.; Iwahori, K.; Miura, A.; Yamane, M.; Yamashita, I. Circularly polarized luminescent CdS quantum dots prepared in a protein nanocage. *Angew. Chem. Int. Ed.* **2010**, *49*, 7006–7009.

[71] Zheng, Y. G.; Yang, Z. C.; Ying, J. Y. Aqueous synthesis of glutathione-capped ZnSe and $Zn_{1-x}Cd_xSe$ alloyed quantum dots. *Adv. Mater.* **2007**, *19*, 1475–1479.

[72] Arslan, I.; Yates, T. J. V.; Browning, N. D.; Midgley, P. A. Embedded nanostructures revealed in three dimensions. *Science* **2005**, *309*, 2195–2198.

[73] Li, H. Y.; Xin, H. L.; Muller, D. A.; Estroff, L. A. Visualizing the 3D internal structure of calcite single crystals grown in agarose hydrogels. *Science* **2009**, *326*, 1244–1247.

[74] Chen, J. L.; Zhu, C. Q. Functionalized cadmium sulfide quantum dots as fluorescence probe for silver ion determination. *Anal. Chim. Acta* **2005**, *546*, 147–153.

[75] Han, B. Y.; Yuan, J. P.; Wang, E. K. Sensitive and selective sensor for biothiols in the cell based on the recovered fluorescence of the CdTe quantum dots-Hg(II) system. *Anal. Chem.* **2009**, *81*, 5569–5573.